CO2 hydrates crystallization kinetic parametric study: effect of stirring rate and impeller type.

Véronique Osswald, Pascal Clain, Anthony Delahaye, L. Fournaison

DOI: 10.18462.iir.pcm.2024.0024

CO_2 HYDRATES CRYSTALLIZATION KINETIC PARAMETRIC STUDY: EFFECT OF STIRRING RATE AND IMPELLER TYPE

Véronique OSSWALD[(1)], Pascal CLAIN[(2, 1)], Anthony DELAHAYE[(1)], Laurence FOURNAISON[(1)]

(1) Université Paris Saclay, INRAE, Frise, 92761 Antony, France
(2) Leonard de Vinci Pôle Universitaire, Research Center, 92916 Paris La Défense, France

ABSTRACT

Carbon dioxide hydrates are ice-like crystalline solids composed of CO_2 molecules trapped inside cages of hydrogen-bonded water molecules. CO_2 hydrate slurries can be used as phase change material for industrial issues of cold distribution due to the high dissociation enthalpy of CO_2 hydrate (around 374 kJ kg^{-1}, higher than that of ice – 333 kJ kg^{-1}). However, the formation rate of CO_2 hydrate is a real limitation, and the way to control and promote it is a key parameter.
The present work investigates the kinetics of CO_2 hydrate crystallization for two different types of stirrers: on the one hand a three-pitched blade stirrer and, on the other hand, a hollow shaft eight-blade Rushton turbine. A jacketed stirred batch reactor, with a specially developed sensor (a thermopile), is used to determine experimental heat balance on the cooling jacket. The mass fraction of crystallized hydrate during the time is determined directly from this heat balance. We conclude with the global performance of both heat and mass transfers of the stirrer and give general recommendations for the choice of stirrer type and scale-up process.

1. INTRODUCTION

Secondary refrigeration consists of using an environmentally friendly fluid for cold distribution and storage to confine primary refrigerants and reduce their quantities, thus reducing their direct greenhouse effect due to gas emissions. CO_2 hydrates slurry is a promising PCM slurry for secondary refrigeration due to the high latent heat (around 374 kJ.kg^{-1}). It can be used in a wide range of temperature conditions suitable for air conditioning applications (see Figure 1).

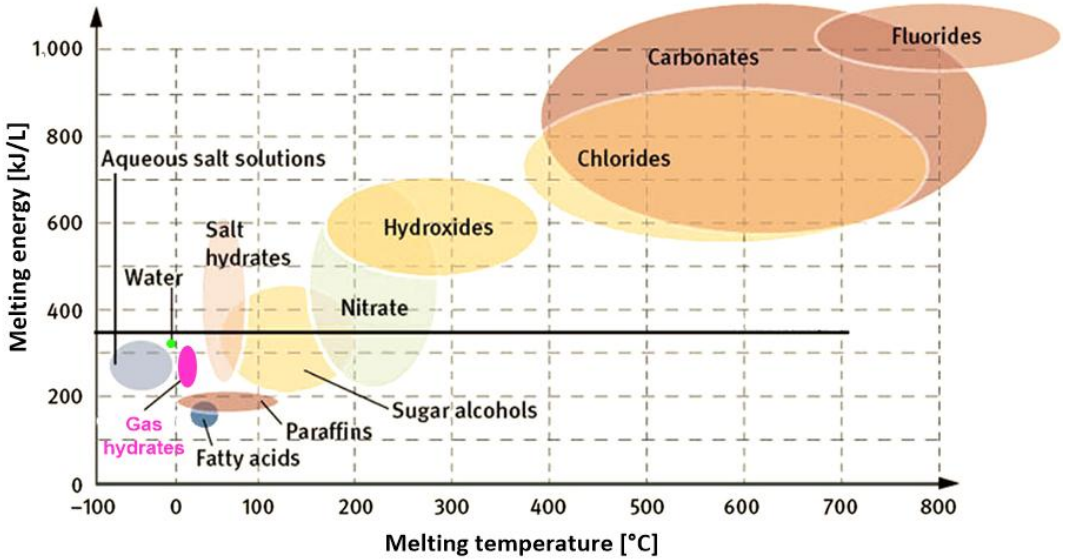

Figure 1: Mapping of potential Phase Change Materials (PCM) based on their melting temperature range and melting enthalpy (according to Mehling and Cabeza (2007))

Clathrate hydrates of CO_2 are ice-like crystalline solids composed of CO_2 molecules trapped inside cages of hydrogen-bonded water molecules. While the thermodynamic properties of CO_2 hydrates are now well established, knowledge of crystallization kinetics phenomena is always a challenge (Warrier *et al.* (2016),

DOI: 10.18462.iir.pcm.2024.0024

Liu *et al.* (2022)). Trying to understand and control gas hydrate formation is a key factor since the discovery of hydrates in pipeline plugs by Hammerschmidt (1934). Most hydrate-based reactors at the laboratory scale are equipped with pressure and temperature recorders. Many kinetic models (Englezos *et al.* (1987a), Englezos *et al.* (1987b), Skovborg and Rasmussen (1994)) are mass balance based on assumptions on CO_2 concentration in the liquid phase and on CO_2 and water molar composition of hydrates. Another method used Differential Thermal Analysis (DTA) (Clain *et al.*, 2015) to determine the formation rate of CO_2 and TBPB hydrate slurries. This study aims to apply a heat balance model to assess CO_2 hydrate formation kinetics in a lab-scale reactor thanks to an original thermopile device installed between the inlet and outlet of the cooling jacket. This method is used to compare intensification parameters: stirring range and stirring type.

2. MATERIAL AND METHOD

2.1. Raw material specifications

A carbon dioxide gas cylinder of 99.995% (by volume) purity purchased from Linde Gas and ultra-pure water type I, obtained from the Milli-Q® water purification system, were used for experiments.

2.2. Equipment

The setup used for those experiments is illustrated in

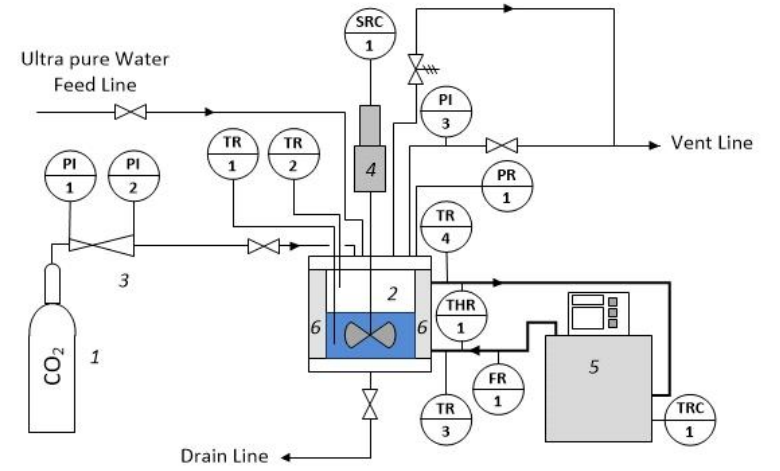

1: CO_2 gas cylinder, *2*: Stirred tank reactor (STR), *3*: Pressure regulator, *4*: Stirrer motor, *5*: Cooling/heating unit, *6*: Cooling/heating jacket

Instrumentation:

FR: Flow recorder; PI: Pressure indicator; PR : Pressure recorder; SIC: Speed indicator controller; TR: Temperature recorder; TRC: Temperature recorder controller; THR thermopile recorder

DOI: 10.18462.iir.pcm.2024.0024

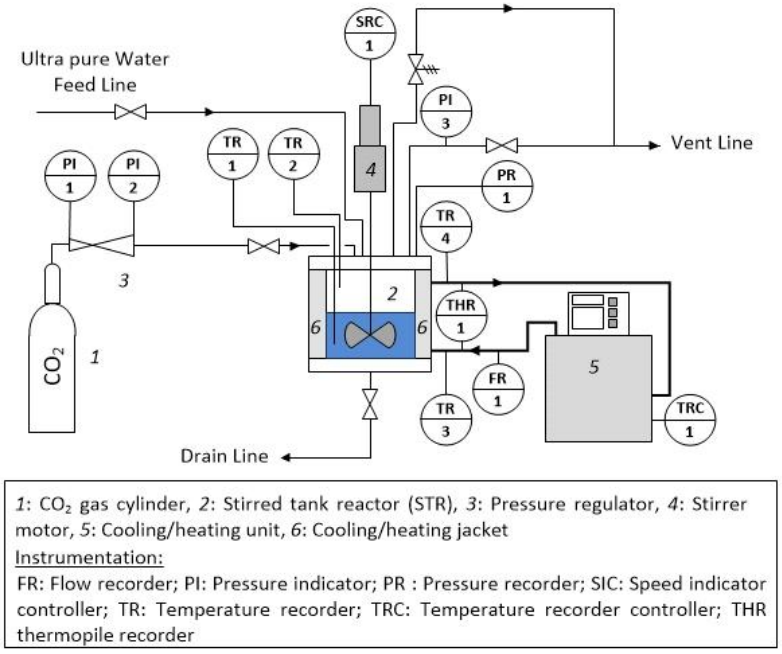

Figure 2: Scheme of the experimental setup

The device comprises four parts: CO_2 feed, an external refrigerating unit, a magnetic drive coupling motor agitator, and a customized stainless steel reactor. The maximum operating pressure of this reactor was 3.8 MPa, with an internal volume of $1.4*10^{-3}$ m^3. The reactor was built with a cooling jacket to control the reactor temperature set-point using a coolant (water + mono propylene glycol). The external cooling/heating unit was a Julabo FP50-HE circulator of 8L capacity with an acceptable temperature stability of 0.01 °C. The cooling capacity of the Julabo FP 50-HE circulator was 0.8 kW. The agitator assembly consisted of a motor, variable frequency motor speed regulator, magnetic drive coupling, suitable drive mounting, shaft, and one of the two propellers described in part 2.2.2. The vessel was equipped with a pressure transmitter supplied by Keller, calibrated at the laboratory, and had an uncertainty of 0.1 % within the range of 0 - 4 MPa. An analog pressure gauge (PI3) was also used to monitor pressure, especially during the depressurization step. The CO_2 injection pressure was controlled by a cylinder pressure regulator supplied by Messer with an outlet pressure range of 0 - 10 MPa. All the temperatures were measured by copper-constantan T-type thermocouples, calibrated at the laboratory, and had an uncertainty of -/+ 0.2 K within the range of 263.15 - 298.15 K. Coolant flow inside the cooling jacket was measured by a Rosemount 8750W magnetic flowmeter supplied by Emerson Process within a range of 0 – 40 L/hr. A special sensor, a thermopile (THR1 see

DOI: 10.18462.iir.pcm.2024.0024

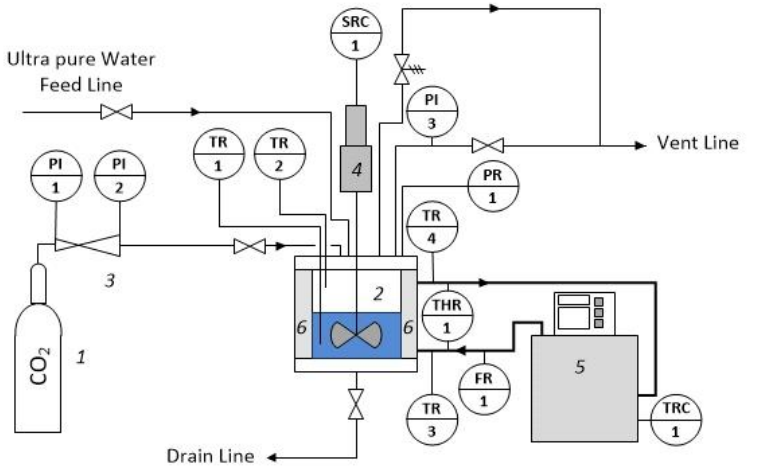

1: CO_2 gas cylinder, *2*: Stirred tank reactor (STR), *3*: Pressure regulator, *4*: Stirrer motor, *5*: Cooling/heating unit, *6*: Cooling/heating jacket

Instrumentation:

FR: Flow recorder; PI: Pressure indicator; PR : Pressure recorder; SIC: Speed indicator controller; TR: Temperature recorder; TRC: Temperature recorder controller; THR thermopile recorder

), has been developed to measure the temperature difference between the outlet and inlet of the cooling jacket. Temperature, pressure, flow, and thermopile recorders are connected to a Data Acquisition system supplied by Agilent and connected to a PC. The monitoring and recording of all process values (temperatures, pressure, flow, heat balance, every 10 s), the control of CO_2 injection, and temperature set-point of the heating/cooling unit were done thanks to a VBA code. The external insulation of the cooling jacket and the reactor bottom side is a 19 mm thick Armacell sheet. The device is located in a cold room to control the environment's temperature, set at 10 °C for this study.

2.2.1. Thermopile detailed description

The thermopile consists of six T-type thermocouples connected in series and distributed as follows: the odd thermocouples are installed at the jacket inlet, and the even thermocouples are installed at the jacket outlet. The thermopile signal was measured between the inlet and outlet side (see Figure 3).

Two other thermocouples are associated with this thermopile to determine the temperature at the reactor jacket's inlet (TR3) and outlet (TR4). The installation of this thermopile is linked to the high uncertainty of the calculated temperature difference (TR4-TR3), which is the same order of magnitude as the value, often less than 0.1°C (see Figure 4).

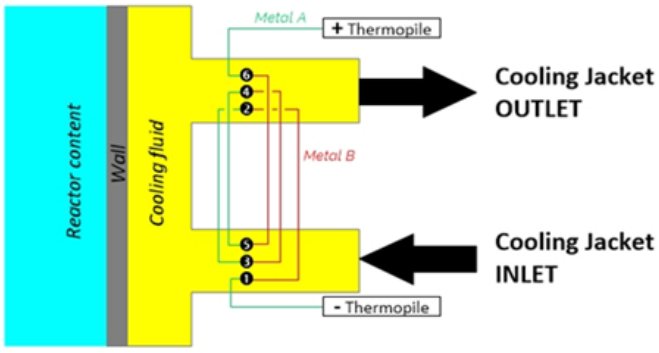

Figure 3: Detailed scheme of thermopile

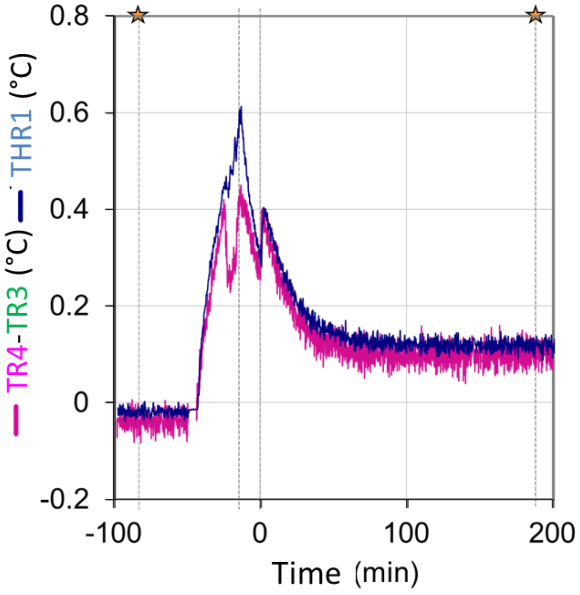

Figure 4: Calculated temperature difference TR4-TR3 and measured thermopile THR1

DOI: 10.18462.iir.pcm.2024.0024

Similarly, the mean and standard deviations were measured and calculated for the inlet and outlet thermocouples and the thermopile measurement. Table 1 presents the standard deviation obtained for each calibration temperature step.

Table 1: Standard deviation of inlet TR3, outlet TR4, calculated difference TR4 – TR3 temperatures, and thermopile THR1 signal during calibration.

Calibration temperature step		-5 °C	0 °C	5 °C	10 °C	15 °C	25 °C
Standard deviation	TR4 (°C)	0.0182	0.0182	0.0153	0.0156	0.0469	0.0182
	TR3 (°C)	0.0226	0.0219	0.0214	0.0219	0.0564	0.0226
	TR4 – TR3 (°C)	0.0214	0.0176	0.0198	0.0193	0.0201	0.0214
	Thermopile THR1 (°C)	0.0035	0.0037	0.0038	0.0040	0.0033	0.0035

The results of Table 1 show that the standard deviation on the outlet-inlet temperature difference is up to four times higher than that of the thermopile.

2.2.2. Stirrer type

Two different types of stirrers were used. On one hand, a three 45° pitched blades impeller (hereafter impeller A); on the other hand, a special Rushton turbine, with eight blades and two discs, equipped with a gas dispersing system, patented under the name Dispersimax (hereafter impeller B). Impeller A is an axial flow impeller, especially suited for solid/liquid application due to its effective suspension of solid particles in the liquid (see Figure 5). Impeller B is a radial flow impeller. It is stirring and simultaneously drawing a gas down through the hollow shaft and dispersing it inside the liquid (see Figure 6).

Figure 5: Impeller A

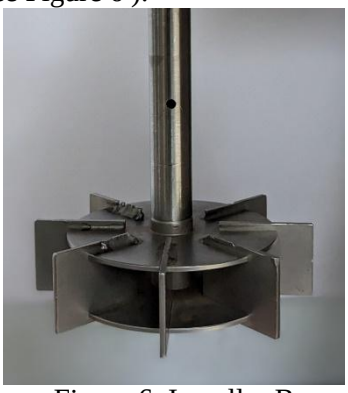

Figure 6: Impeller B

2.3. Experimental protocol

The initial temperature reactor set point was chosen at least 12 °C to avoid the risk of CO_2 hydrate formation during gas injection. The reactor was filled with 0.7 kg of ultrapure water. This study chose this water load to achieve a gas-to-liquid volume ratio of 1:1. After setting the stirring speed (speed set-point of the stirrer ranged between 100 and 760 rpm), the air inside the reactor was removed with a vacuum pump. It allows for degassing any CO_2 naturally dissolved in the water upon contact with the air. Then the reactor was fed with CO_2 and part of it was dissolved in water. The amount of gas injected inside the reactor depends on the expected operating conditions (temperature and final hydrates mass fraction). The crystallization process comprises four successive key points marked by the letters A, B, C, and D (see Figure 7 and Figure. Point A corresponds to the system's initial state after CO_2 injection and before cooling, when the dissolution thermodynamic equilibrium is reached. Point B represents when the system's pressure and temperature have reached thermodynamic conditions that allow hydrate crystallization (see Figure). However, the system is in a metastable liquid-vapor state between B and C without hydrate crystals. Point C corresponds to the rupture of supercooling. Between C and D, hydrates crystallize. Point D corresponds to the system's final state imposed by the jacket temperature set. In the following results and discussion part, the first experimental result shows those key points.

DOI: 10.18462.iir.pcm.2024.0024

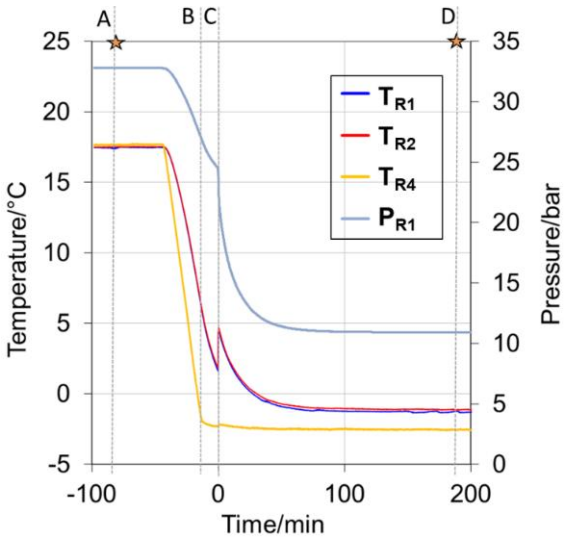

Figure 7: Temperatures and pressure vs time

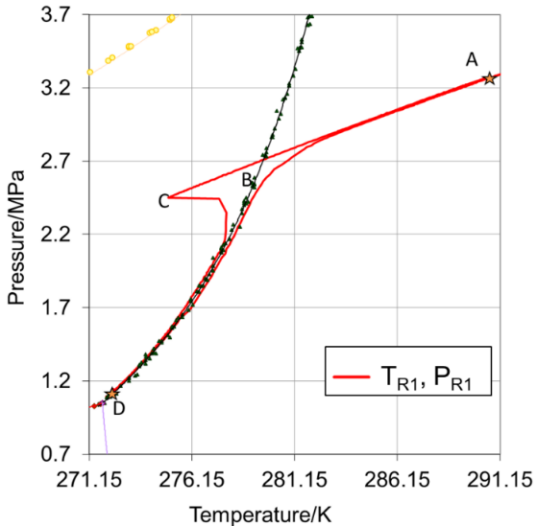

Figure 8: Thermodynamic P, T diagram

3. RESULTS AND DISCUSSION

3.1. Stirring rate effect

This section examines the influence of stirring rate on the CO_2 hydrate formation kinetics. Propeller A was employed for this investigation, with four rates tested: 100, 420, 610, and 760 RPM. The final amount of hydrates expected is around 12% wt.

DOI: 10.18462.iir.pcm.2024.0024

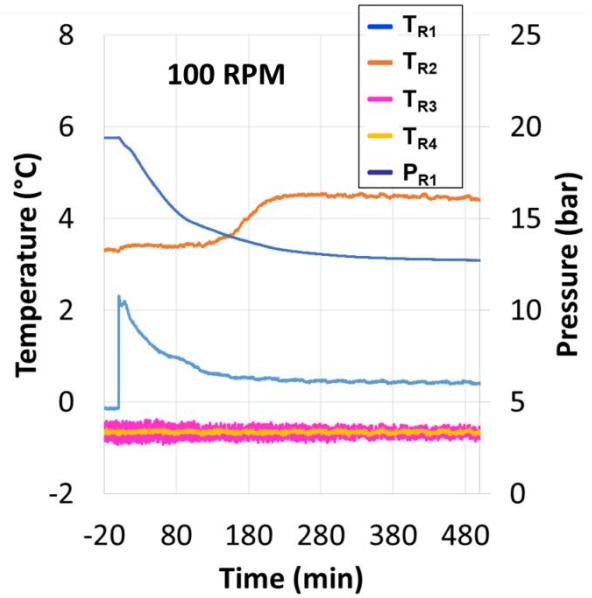

Figure 9: Temperatures (TR1; TR2), pressure (PR1) inside the reactor and inlet (TR3)/ outlet(TR4) temperatures of cooling jacket – 100 RPM

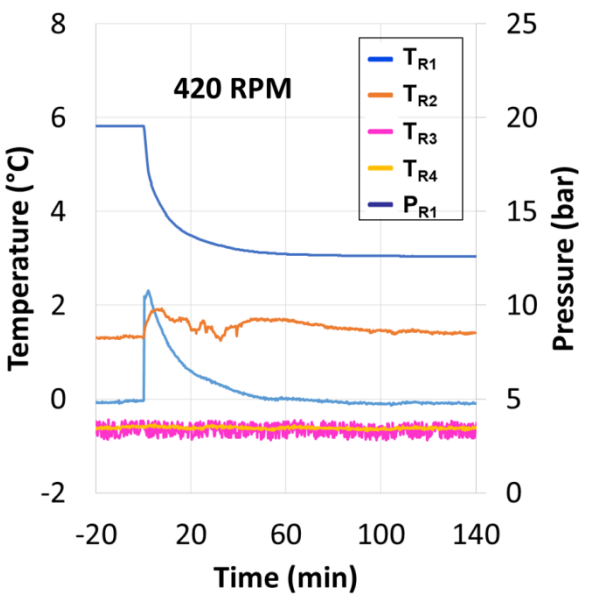

Figure 10: Temperatures (TR1; TR2), pressure (PR1) inside the reactor and inlet (TR3)/ outlet(TR4) temperatures of cooling jacket – 420 RPM

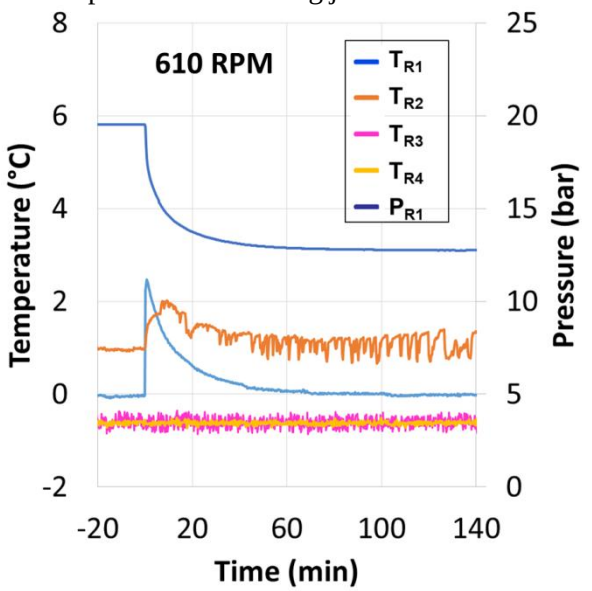

Figure 11: Temperatures (TR1; TR2), pressure (PR1) inside the reactor and inlet (TR3)/ outlet(TR4) temperatures of cooling jacket – 610 RPM

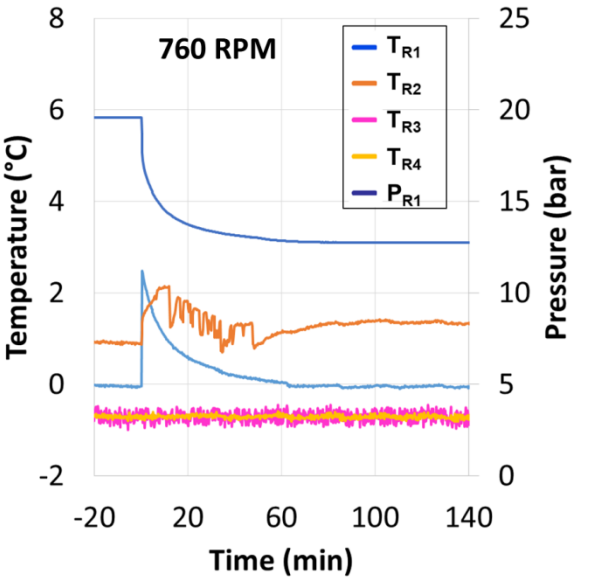

Figure 12: Temperatures (TR1; TR2), pressure (PR1) inside the reactor and inlet (TR3)/ outlet(TR4) temperatures of cooling jacket – 760 RPM

Figures 9, 10, 11, and 12 show the evolution during the time of temperatures inside the liquid phase TR1, inside the vapor phase TR2, at the inlet TR3, and at the outlet TR4 of the cooling jacket, and the pressure PR1 inside the reactor respectively at 100, 420, 610 and 760 RPM. The initial conditions were the same for the four tests and the final set-point temperature of the cooling bath too (- 0.7 °C). There are significant similarities in the shapes of the formation profiles at 420, 610, and 760 RPM, unlike at 100 RPM, especially the pressure drop inside the reactor. The time required to form the total amount of hydrates is significantly longer at 100 RPM than at the other three speeds (more than three times longer). The temperatures of both the vapor and liquid/slurry phases are also affected. The vapor phase temperature reaches 4.5°C at 100 RPM compared to 1.5°C for the other speeds. For the final temperature of the liquid phase, at the end of crystallization, it is 0.5°C higher at 100 RPM compared to the other speeds.

DOI: 10.18462.iir.pcm.2024.0024

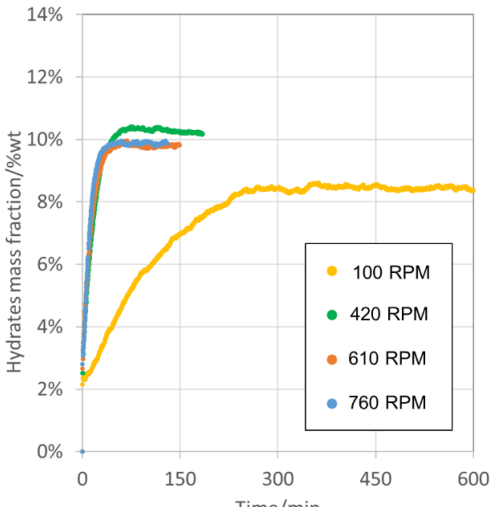

Figure 13: Hydrates mass fraction vs. time for 100, 420, 610 and 760 RPM

Figure 13 illustrates the evolution of crystallized hydrate mass fraction over time for the four speeds. These curves were obtained using the thermal model and the following assumptions:

- Integration of the area under the power curve was calculated via thermopile between two instants, t and t+dt, to determine the heat transferred by the slurry and received by the cooling jacket.
- The slurry absorbs the heat released by the crystallization of hydrate crystals during dt. A part of it is accumulated within the slurry, leading to a temperature increase of the slurry.

As seen at 100 RPM, the final estimated quantity of hydrates is 1.5%wt lower than for the other three speeds. In conclusion, at 100 RPM, mass and heat transfer are poor, limiting the total amount of crystallized hydrates. Moreover, the kinetic is significantly slower. Let's now focus on the impact of agitation device type on kinetics enhancement.

3.2. Stirring type effect

The experiments were conducted at 610 RPM to compare propellers A and B to ensure that the speed effect does not limit the results. The final amount of hydrates expected is 20%wt.

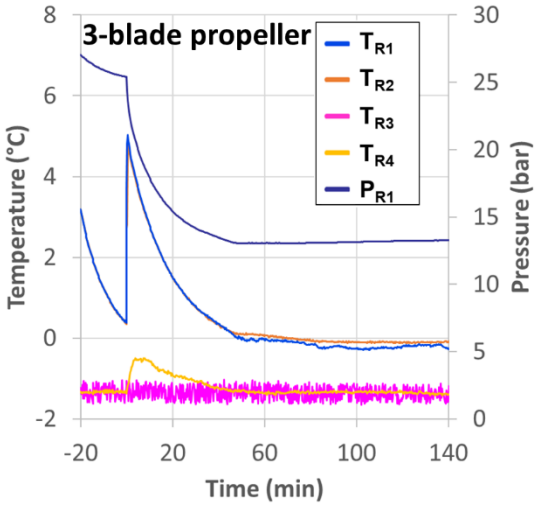

Figure 14: Temperatures and pressure vs time – Impeller A 610 RPM

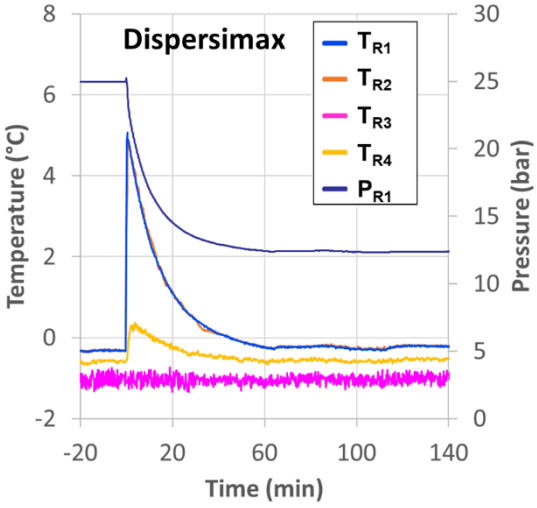

Figure 15: Temperatures and pressure vs time – Impeller B 610 RPM

Figures 14 and 15 show the evolution during the time of temperatures inside the liquid phase TR1,inside the vapor phase TR2, at the inlet TR3 and the outlet TR4 of the cooling jacket, and the pressure PR1 inside the reactor, respectively, with impeller A and B at 610 RPM. The initial conditions were the same for the two tests, and the final set-point temperature of the cooling bath, too (- 1.3 °C). In contrast to the previous experiments (see Figures 9, 10, 11, and 12), the temperatures of the vapor and liquid phases are overlapped. The final temperature TR1 and the final pressure PR1 were slightly lower for impeller B than for impeller A.

DOI: 10.18462.iir.pcm.2024.0024

This suggests that the final amount of hydrates obtained with impeller B will be higher than that obtained with impeller A.

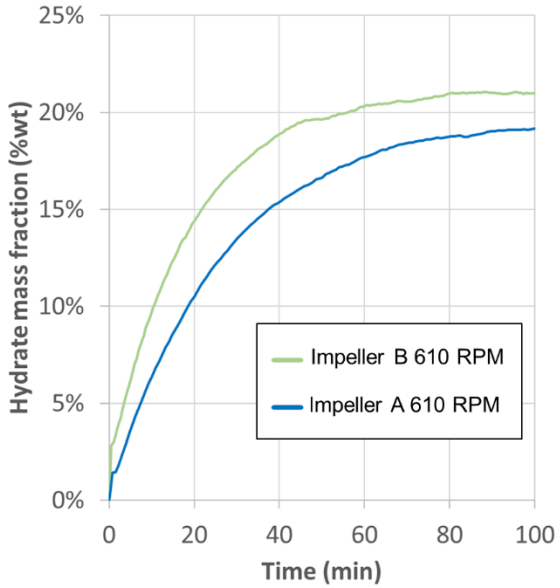

Figure 16: Hydrates mass fraction vs. time - comparison between impellers A and B

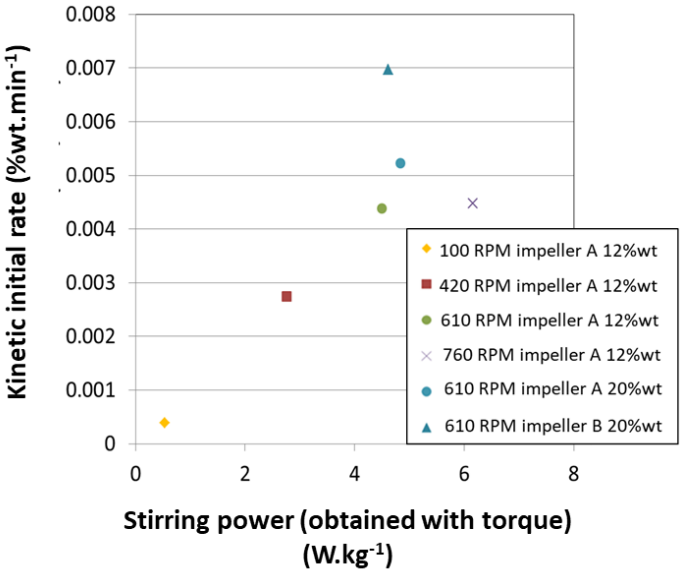

Figure 17: Initial kinetic rate vs. stirring power

Figure 16 shows the evolution of the hydrate mass fraction obtained during the test for both impellers. The kinetics observed with impeller B are faster than those observed with impeller A. Additionally, the final hydrate fraction obtained with impeller B is higher than that obtained with impeller A. The crystallization process is enhanced with impeller B, suggesting that vapor-liquid mass transfer is a limiting step. Figure 17 represents the initial kinetic rates of crystallization as a function of consumed agitation power. Firstly, regarding the experiments on the effect of agitation speed, it is noted that there is no significant gain in kinetics beyond 610 RPM. Secondly, comparing the agitation devices shows that impeller B outperforms impeller A even for the initial kinetic rate.

4. CONCLUSION

For this study, a specific device equipped with a direct temperature difference measurement between the inlet and outlet of the cooling jacket was developed and validated. An investigation was performed into the effect of agitation speed and the type of agitation device on the hydrate crystallization kinetics. In the case of impeller A at 100 RPM, both mass and heat transfer were less significant than at speeds above 420 RPM. It was also demonstrated that impeller B intensified crystallization more than impeller A at the same agitation rate and that the limiting step was vapor/liquid transfer. The volumetric mass transfer coefficient, k_La, is a parameter that describes the rate at which a gaseous compound CO_2 can transfer between the vapor and liquid phases. Future measurements of the k_La could further confirm this.

5. ACKNOWLEDGMENT

This work was supported by the French National Research Agency under the program COOLHYD (ANR-22-CE50-0001) and undertaken in the frame of the French Research Consortium “GDR-2026 Hydrates de gaz”.

6. REFERENCES

Mehling, H.,Cabeza, L. F., 2007. Phase Change Materials and their basic properties. *Thermal Energy Storage for Sustainable Energy Consumption*, Springer Netherlands, 257-277.

DOI: 10.18462.iir.pcm.2024.0024

Warrier, P., Khan, M. N., Srivastava, V., Maupin, C. M.,Koh, C. A., 2016. Overview: Nucleation of clathrate hydrates. *J. Chem. Phys.* 145 (21).

Liu, F.-P., Li, A.-R., Qing, S.-L., Luo, Z.-D.,Ma, Y.-L., 2022. Formation kinetics, mechanism of CO_2 hydrate and its applications. *Renewable and Sustainable Energy Reviews* 159, 112221.

Hammerschmidt, E. G., 1934. Formation of Gas Hydrates in Natural Gas Transmission Lines. *Ind. Eng. Chem.* 26 (8), 851-855.

Englezos, P., Kalogerakis, N., Dholabhai, P. D.,Bishnoi, P. R., 1987a. Kinetics of formation of methane and ethane gas hydrates. *Chem. Eng. Sci.* 42 (11), 2647-2658.

Englezos, P., Kalogerakis, N., Dholabhai, P. D.,Bishnoi, P. R., 1987b. Kinetics of gas hydrate formation from mixtures of methane and ethane. *Chem. Eng. Sci.* 42 (11), 2659-2666.

Skovborg, P.,Rasmussen, P., 1994. A mass transport limited model for the growth of methane and ethane gas hydrates. *Chem. Eng. Sci.* 49 (8), 1131.

Clain, P., Osswald, V., Spiga, O., Delahaye, A.,Fournaison, L., 2015. A new formation kinetic study method of TBPB and CO_2 hydrates based on DTA. Une nouvelle méthode d'étude cinétique de formation des hydrates de TBPB et de CO_2 basée sur l'ATD. *24th IIR International Congress of Refrigeration (ICR 2015)*, 8.